# External control of the Drosophila melanogaster egg to imago development period by specific combinations of 3D low-frequency electric and magnetic fields

**Article** *in* Electromagnetic Biology and Medicine · September 2014

DOI: 10.3109/15368378.2014.959175 · Source: PubMed



**2 authors:**

Vladimir I. Makarov
University of Puerto Rico at Rio Piedras
**165** PUBLICATIONS **737** CITATIONS
SEE PROFILE

Igor Khmelinskii
Universidade do Algarve
**263** PUBLICATIONS **2,175** CITATIONS
SEE PROFILE

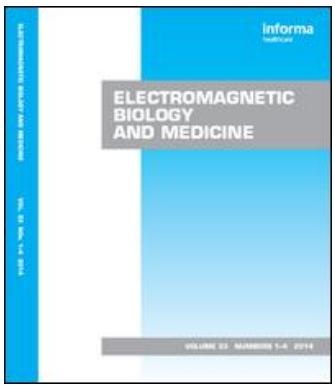


Electromagnetic Biology and Medicine
Publication details, including instructions for authors and subscription information:
http://www.tandfonline.com/loi/iebm20

# External control of the Drosophila melanogaster egg to imago development period by specific combinations of 3D low-frequency electric and magnetic fields

Vladimir I. Makarov[a] & Igor Khmelinskii[b]
[a] Department of Physics, University of Puerto Rico, Rio Piedras, San Juan, PR, USA and
[b] FCT, DQF, and CIQA, Universidade do Algarve, Faro, Portugal
Published online: 26 Sep 2014.



To cite this article: Vladimir I. Makarov & Igor Khmelinskii (2014): External control of the Drosophila melanogaster egg to imago development period by specific combinations of 3D low-frequency electric and magnetic fields, Electromagnetic Biology and Medicine, DOI: 10.3109/15368378.2014.959175

To link to this article: http://dx.doi.org/10.3109/15368378.2014.959175

ELECTROMAGNETIC BIOLOGY AND MEDICINE

http://informahealthcare.com/ebm
ISSN: 1536-8378 (print), 1536-8386 (electronic)

Electromagn Biol Med, Early Online: 1–15
 DOI: 10.3109/15368378.2014.959175

informa healthcare

ORIGINAL ARTICLE

# External control of the *Drosophila melanogaster* egg to imago development period by specific combinations of 3D low-frequency electric and magnetic fields

Vladimir I. Makarov[1] and Igor Khmelinskii[2]

[1]*Department of Physics, University of Puerto Rico, Rio Piedras, San Juan, PR, USA and* [2]*FCT, DQF, and CIQA, Universidade do Algarve, Faro, Portugal*

**Abstract**

We report that the duration of the egg-to-imago development period of the *Drosophila melanogaster*, and the imago longevity, are both controllable by combinations of external 3-dimensional (3D) low-frequency electric and magnetic fields (LFEMFs). Both these periods may be reduced or increased by applying an appropriate configuration of external 3D LFEMFs. We report that the longevity of *D. melanogaster* imagoes correlates with the duration of the egg-to-imago development period of the respective eggs. We infer that metabolic processes in both eggs and imago are either accelerated (resulting in reduced time periods) or slowed down (resulting in increased time periods). We propose that external 3D LFEMFs induce electric currents in live systems as well as mechanical vibrations on sub-cell, whole-cell and cell-group levels. These external fields induce media polarization due to ionic motion and orientation of electric dipoles that could moderate the observed effects. We found that the longevity of *D. melanogaster* imagoes is affected by action of 3D LFEMFs on the respective eggs in the embryonic development period (EDP). We interpret this effect as resulting from changes in the regulation mechanism of metabolic processes in *D. melanogaster* eggs, inherited by the resulting imagoes. We also tested separate effects of either 3D electric or 3D magnetic fields, which were significantly weaker.

**Keywords**

Eggs, egg transformation time, *Drosophila melanogaster*, three-dimensional low-frequency electric and magnetic fields (3D LFEMFs)

**History**

Received 8 June 2014
Revised 19 August 2014
Accepted 25 August 2014
Published online 26 September 2014



## Introduction

External control of biological system dynamics is a very important fundamental and biotechnological problem (Makarov and Khmelinskii, 2013). External control may be performed by way of external conditions (temperature, pressure, electromagnetic fields, magnetic and electric fields, etc.) that affect live systems. Presently, we shall discuss effects of combinations of external three-dimensional low-frequency electric and magnetic fields (3D LFEMFs) on live systems. 3D EMFs are electric and/or magnetic fields with three Cartesian components, each varying in time at its own frequency, presently in the sonic frequency range. Earlier we explored the effects of 3D LFEMFs on different processes in live systems, including cell population growth rates (Makarov and Khmelinskii, 2011), rehabilitation rates of damaged rat eye retina (Makarov, 2013), and the duration of the imago development period of *D. melanogaster* (Makarov and Khmelinskii, 2013).

The effects of external electromagnetic fields on *D. melanogaster* have been extensively studied earlier (Atli and Unlü, 2006; Dalgic, 2003; Onder and Bozcuk, 2004; Panagopoulos et al., 2004; Pay et al., 1978; Ramirez et al., 1983; Tipping et al., 1999; Walters et al., 1987). Pay et al. (1978) investigated the effects of long-term 2450 MHz EMF on reproduction of *D. melanogaster*, finding that EMF exposure reduced the egg production among the females, as compared to control. Pulsed radiofrequency (RF) EMFs from common GSM (global system for mobile telecommunications) telephones with the carrier frequency at 900 MHz has decreased the reproductive capacity of *D. melanogaster* by 50–60%, whereas the same but non-modulated field (non-speaking emission) has decreased the reproductive capacity by only 15–20% (Panagopoulos et al., 2004), underlining the important contribution of acoustic frequencies. Similarly, Ramirez et al. (1983) observed that oviposition in *D. melanogaster* was reduced by exposure to extremely low frequency (ELF) pulsed fields (100 Hz, 1.76 mT) and sinusoidal fields (50 Hz, 1 mT). In contrast, it was reported that 50 Hz and 8 mT EMF exposure had no discernible effect when third-stage larvae were exposed (Tipping et al., 1999). In a similar work, Walters et al. (1987) reported that 60 Hz magnetic fields did not affect egg production of *D. melanogaster*. Atli and Unlü (2006) also studied the effects of microwave-frequency electromagnetic fields (EMF) on the fecundity of *D. melanogaster*. The Oregon strain

Address correspondence to Professor Vladimir Ivanovich Makarov, University of Puerto Rico, Department of Physics, Rio Piedras, Campus, PO Box 23343, San Juan, PR 00931, USA. Tel: +1 787 529 2010. E-mail: vmvumakarov@gmail.com; vladimir.makarov@uprrp.edu

females were exposed to 10 GHz EMFs continuously (3, 4 and 5 h) and discontinuously (3 h exposure + 30 min interval + 3 h exposure). The fecundity in the 4 and 5 h exposed groups was significantly reduced as compared to the control ($p < 0.05$). There was a reduction in the 3 h and 3 + 3 h exposed groups, although not as significant ($p > 0.05$). We shall reassess these and other studies in the ''Discussion'' section.

Presently we continue the studies of 3D LFEMF effects on the egg-to-imago development period duration and its correlation with the imago longevity in *D. melanogaster*. We use combinations of 3D LFEMFs in the audible sound frequency range and up to 30 kHz. We report experimental studies of these parameters controlled by combination of external 3D LFEMFs, including their detailed field dependences and correlations. We identified specific sets of the 3D LFEMF parameters for the *D. melanogaster* eggs, whereby we could either increase (the first parameter set) or reduce (the second parameter set) their egg-to-imago development period (EDP). We also found correlations between the effects on the EDP and the imago longevity in *D. melanogaster*. These results may be used in biomedical and medical applications. In a future study, we shall use biophysical and biochemical methods to investigate the detailed mechanisms of 3D LFEMF action on live systems.

## Materials and methods

The experimental setup described earlier was partially used in the present study (Makarov, 2013; Makarov and Khmelinskii, 2011, 2013).

### *D. melanogaster* egg preparation

The eggs were collected between 2 and 4 h after oviposition and 100 eggs were used in each of the experiments. The sets of eggs were exposed in the 3D LFEMF cell, described below in detail. We used the same cell in separate experiments with either magnetic or electric field components switched off.

The *D. melanogaster* eggs were prepared as follows. First, we joined 100 males and 100 females with 6–8 h age after emergence (Roberts, 1998) in a $30 \times 30 \times 30\,cm^3$ plastic box with excess food [recipe by Wheeler and Clayton (1965) amended by Bozcuk (1978) and King (1970)] kept at $25 \pm 1\,^{\circ}C$ with a slow air flow at $70 \pm 1\%$ humidity passing through and in 8 h light, 16 h dark periods in otherwise standard conditions (Bozcuk, 1978; Roberts, 1998). Standard *D. melanogaster* (common fruit fly) was used. The box was incubated during 2–4 h, after which all *D. melanogaster* eggs were collected. Each of the experiments used 100 eggs. The eggs were selected by size ($0.18 \pm 0.06$ mm width; $0.51 \pm 0.10$ mm length).

### Experimental cell

The experimental 3D LFEMF cell has been described in detail earlier (Makarov and Khmelinskii, 2013). The cell includes a plastic box $15 \times 15 \times 15\,cm^3$ internal size, coils (15 cm internal diameter) to produce periodic magnetic fields, and circular planar electrodes (14 cm diameter) to produce periodic electric fields. The cell is schematically shown in Figure 1. Periodic magnetic and electric fields were created in the zone where the biological samples were located:

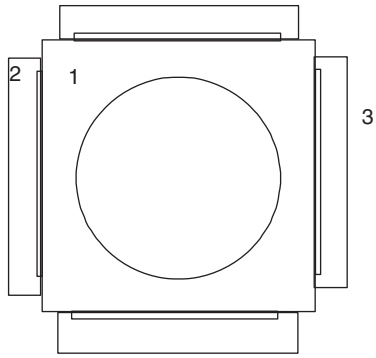


Figure 1. 3D LFEMF cell: (1) is the plastic box ($15 \times 15 \times 15\,cm^3$ of the internal volume); (2) wire coils to produce variable magnetic field $B_i = B_{i,0}Cos(\omega_i t + \phi_i)$, where the amplitude $B_{i,0}$ was up to 15 G; (3) circular planar electrodes to produce variable electric field $D_j = D_{j,0}Cos(\omega_j t + \phi_j)$, where the amplitude $D_{j,0}$ was up to 15 V/cm.

$$B_i = B_{i,0}\,Cos(\omega_i t + \varphi_i) \tag{1}$$

$$D_j = D_{j,0}\,Cos(\omega_j t + \varphi_j) \tag{2}$$

where $i, j = x, y, z$, $B_{i,0}$ and $D_{j,0}$ are magnetic and electric field inductions, $\omega_i$ and $\omega_j$ are harmonic frequencies of the magnetic and electric induction oscillations, $\varphi_i$ and $\varphi_j$ are phases of the magnetic and electric field inductions. All of the field parameters could be chosen as required, with $B_{i,0}$ from 0 to 15 G and $D_{j,0}$ from 0 to 15 V/cm; $\omega_i$ and $\omega_j$ – 10 to 30,000 Hz; $\varphi_i$ and $\varphi_j$ – 0 to $2\pi$. The exposure time was also chosen as required.

According to the Maxwell equations presented in SGS units:

$$\frac{\partial \vec{D}}{\partial t} = rot(\vec{B}), \tag{3}$$

$$\frac{\partial \vec{B}}{\partial t} = -rot(\vec{D}), \tag{4}$$

time-variable electric and magnetic fields induce secondary magnetic and electric fields. For example, the $x$ components of these secondary fields are given by:

$$\frac{\partial B_x}{\partial t} = \left(\frac{\partial D_y}{\partial z} - \frac{\partial D_z}{\partial y}\right)$$
$$\frac{\partial D_x}{\partial t} = -\left(\frac{\partial B_y}{\partial z} - \frac{\partial B_z}{\partial y}\right) \tag{5}$$

In general, we may write:

$$\frac{\partial \vec{X}}{\partial t} = \pm \begin{vmatrix} i & j & k \\ X_x & X_y & X_z \\ \dfrac{\partial}{\partial x} & \dfrac{\partial}{\partial y} & \dfrac{\partial}{\partial z} \end{vmatrix} \tag{6}$$

where $X = D$ or $B$, the plus sign is to be used for time derivatives of $B$, and the minus sign for the time derivative of $D$. Using Equation (4), we estimated the strength of the induced magnetic and electric fields in the active area of

the 3D LFEMF cell. The estimated maximum values of the induced secondary field amplitudes in the cell center are 0.081 G and 0.014 V/cm, respectively. Thus, we neglected these induced fields in any further considerations.

The 3D LFEMF cell was built around a cubic plastic chamber, manufactured of polymethylmethacrylate plates 1.0 cm thick, plate size: $17 \times 17$ cm (2 plates), $17 \times 15$ cm (2 plates) and $15 \times 15$ cm (2 plates). The volume of the sample chamber was *ca*. 3375 $cm^3$. Six planar stainless-steel circular electrodes were placed inside the chamber as it is shown in Figure 1. The distance between the two electrodes in a pair was 15 cm. Three pairs of coils were mounted outside of the chamber; with the 17 cm distance between the opposite coils being equal to the coil diameter. Three independent voltage generators were used to create 3D LF electric fields (3D LFEFs) in the chamber, each producing an output voltage varying according to the expression

$$U = a \times Cos(\omega_a t + \varphi_a) \quad (7)$$

where amplitude $a$, cyclic frequency $\omega_a$ and phase $\varphi_a$ could be appropriately controlled, with the maximum voltage amplitude of 225 V. The generators were implemented using a PC computer, a *Keithley* KPCI-1800 I/O board, and a home-made multichannel voltage amplifier. Similarly, three independent current generators were used to create periodic 3-D LF magnetic fields (3D LFMFs) in the active zone of the chamber, each producing an electric current varying according to the expression

$$I = b \times Cos(\omega_b t + \varphi_b) \quad (8)$$

where amplitude $b$, cyclic frequency $\omega_b$ and phase $\varphi_b$ could be appropriately controlled, with the maximum current amplitude of 5 A, equivalent to the maximum magnetic field value of $1.5 \times 10^{-3}$ T in the central zone of the chamber. These generators were implemented in the same way as the voltage generators and used home-made current amplifiers. All of the six generators were operated via a home-made computer program running in the LABVIEW software environment, whereby the desired configuration of 3D periodic electromagnetic field was set. Summing the three Cartesian components, we could achieve up to $2.6 \times 10^{-3}$ T periodic magnetic field and up to 2.6 V/cm periodic electric field, with the fields essentially homogeneous within the active zone of the cell where the *D. melanogaster* eggs were located. Note that the electric and magnetic field homogeneity within the 5 cm diameter central zone was 0.6%, although the effects were much more strongly dependent on frequencies than on amplitudes. The magnetic field was measured using a Hall sensor and a digital oscilloscope (LeCroy). All of the experiments were carried out at a stabilized temperature of $25 \pm 1$ °C using a commercial incubator (Memmert Inc., model IF30PLUS), modified to accommodate the experimental cell, and allowing for visual control of the *D. melanogaster* population.

### *Experiments on egg samples*

Control sets of *D. melanogaster* eggs were kept unexposed to any external EMFs. Test sets were exposed to 3D LFEMFs during specified time, with a new egg set used for each configuration of the external 3D LFEMFs. The number of emergent imagoes was determined each 8 h from the beginning of the experiment and each 0.5 h after the emergence of the first imago. The results are presented as histograms to facilitate analysis, with each of the data points obtained by averaging over 10 independent experiments.

### *Experiments on* D. melanogaster *males*

First, 50 *D. melanogaster* males were selected from populations produced in section (*i*). The longevity of the imagoes was measured as detailed earlier (Makarov and Khmelinskii, 2013), with the number of dead imagoes determined each 8 h from the beginning of the experiment and each 1 h during the imago life period, thus we were using two different time scales. The results were similarly presented as histograms, with each of the data points obtained by averaging of 10 independent experiments.

### *Exposure conditions*

All of the experiments were carried out in the same experimental conditions: 25 °C temperature, $70 \pm 1$% humidity, 8 h light and 16 h dark periods per day, in otherwise standard conditions. No special measures were taken to compensate for the geomagnetic field. Control sets of eggs were placed into the incubator and the duration of the egg-to-imago development period was controlled by the number of imagoes that have emerged. The sets of eggs to be exposed were placed into the EMF cell, exposed for a certain time, transferred into the incubator, and the duration of the egg-to-imago development period was similarly controlled.

## Results

### Experiments on *D. melanogaster* eggs

Egg samples were exposed to EMFs immediately after they were collected, with 5 h exposure time. According to the published development schedules of unexposed eggs (Brody, 1996), the exposure started at Bownes stage 5–8, and ended at stage 11–12 (stages 6–11, on average). No attempt was made to identify the actual development stages in the exposed egg samples. However, according to Panagopoulos (2012), the life cycle of *D. melanogaster* simplified by omitting some intermediate steps may also be presented as shown in Table 1.

Thus, according to this classification, the exposure to EMFs was administered during the oogenesis phase. Possible mechanisms of EMF effects will be discussed below.

The samples were exposed to different configurations of external EMFs. We found that for the same EMF parameter

Table 1. Life cycle of *D. melanogaster* and the duration of phases.

| Life phase | Duration |
|---|---|
| Oogenesis | 48 h |
| Fertilized egg (embryogenesis) | 24 h |
| First instar larva | 24 h |
| Second instar larva | 24 h |
| Third instar larva | 48 h |
| Pupa | 4 d |
| Imago | 20–25 d |

Table 2. Values of the 3D LFEMF parameters that reduce (negative effect) or increase (positive effect) the EDP duration of the *D. melanogaster* eggs.

(a) *Control experiment, reproduced* 10 *times on separate sets of D. melanogaster eggs*

| Parameters | $D_{0,x}$ (V/cm) | $D_{0,y}$ (V/cm) | $D_{0,z}$ (V/cm) | $\omega_{ex}$ (Hz) | $\omega_{ey}$ (Hz) | $\omega_{ez}$ (Hz) | $\varphi_{ex}$ (rad) | $\varphi_{ey}$ (rad) | $\varphi_{ez}$ (rad) |
|---|---|---|---|---|---|---|---|---|---|
| Value | 0 | 0 | 0 | 0 | 0 | 0 | 0 | 0 | 0 |
| Parameters | $B_{0,x}$ (G) | $B_{0,y}$ (G) | $B_{0,z}$ (G) | $\omega_{hx}$ (Hz) | $\omega_{hy}$ (Hz) | $\omega_{hz}$ (Hz) | $\varphi_{hx}$ (rad) | $\varphi_{hy}$ (rad) | $\varphi_{hz}$ (rad) |
| Value | 0 | 0 | 0 | 0 | 0 | 0 | 0 | 0 | 0 |

(b) *Negative effect, reproduced* 10 *times on separate sets of D. melanogaster eggs: the P1 parameter set*

| Parameters | $D_{0,x}$ (V/cm) | $D_{0,y}$ (V/cm) | $D_{0,z}$ (V/cm) | $\omega_{ex}$ (Hz) | $\omega_{ey}$ (Hz) | $\omega_{ez}$ (Hz) | $\varphi_{ex}$ (rad) | $\varphi_{ey}$ (rad) | $\varphi_{ez}$, (rad) |
|---|---|---|---|---|---|---|---|---|---|
| Value | 12.5 | 11.5 | 7.0 | 17,000 | 12,550 | 15,750 | 0 | 0.1 | 0.2 |
| Parameters | $B_{0,x}$ (G) | $B_{0,y}$ (G) | $B_{0,z}$ (G) | $\omega_{hx}$ (Hz) | $\omega_{hy}$ (Hz) | $\omega_{hz}$ (Hz) | $\varphi_{hx}$ (rad) | $\varphi_{hy}$ (rad) | $\varphi_{hz}$ (rad) |
| Value | 9.5 | 13.5 | 11.5 | 20,500 | 15,320 | 22,350 | 0 | 0.8 | 0.7 |

(c) *Positive effect, reproduced* 10 *times on separate sets of D. melanogaster eggs: the P2 parameter set*

| Parameters | $D_{0,x}$ (V/cm) | $D_{0,y}$ (V/cm) | $D_{0,z}$ (V/cm) | $\omega_{ex}$ (Hz) | $\omega_{ey}$ (Hz) | $\omega_{ez}$ (Hz) | $\varphi_{ex}$ (rad) | $\varphi_{ey}$ (rad) | $\varphi_{ez}$, (rad) |
|---|---|---|---|---|---|---|---|---|---|
| Value | 11.5 | 12.5 | 15.0 | 27,000 | 22,550 | 12,750 | 0 | 0.3 | 0.5 |
| Parameters | $B_{0,x}$ (G) | $B_{0,y}$ (G) | $B_{0,z}$ (G) | $\omega_{hx}$ (Hz) | $\omega_{hy}$ (Hz) | $\omega_{hz}$ (Hz) | $\varphi_{hx}$ (rad) | $\varphi_{hy}$ (rad) | $\varphi_{hz}$ (rad) |
| Value | 6.5 | 11.5 | 12.5 | 30,500 | 39,350 | 14,350 | 0 | 0.2 | 0.4 |

The collected data were statistically analyzed using the usual relations, and the comparison with the control experiments was done using the Student's *t*-test. The results are shown in Figure 2 as histograms.



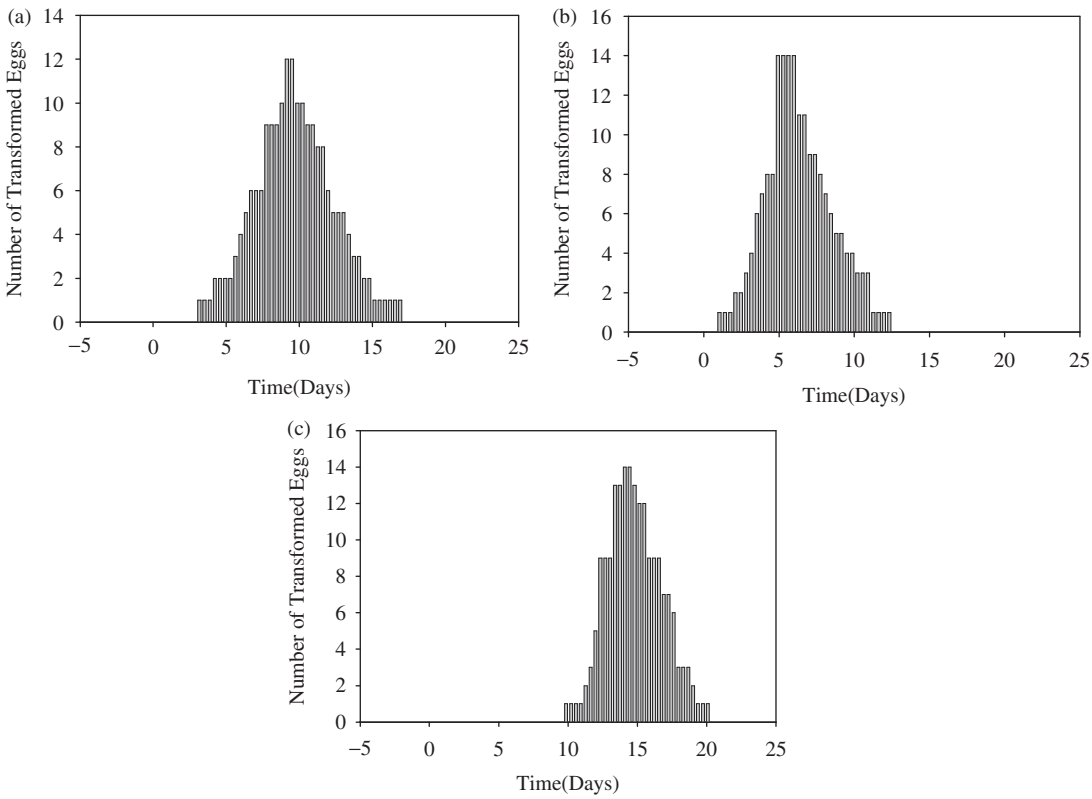


Figure 2. Time-distribution histograms of egg–imago development period (EDP) duration of *D. melanogaster* eggs: (a) the control experiment, reproduced 10 times, refer Table 1; (b) negative effect, reproduced 10 times with separate sets of *D. melanogaster* eggs, refer Table 2; (c) positive effect, reproduced 10 times with separate sets of *D. melanogaster* eggs, refer Table 2.

sets that were identified earlier (Makarov and Khmelinskii, 2013) and presented in Table 2, the histograms were shifted to shorter and longer EDP durations, respectively, as compared to the histogram describing the EDP duration of the control sets of *D. melanogaster* eggs.

The time distributions were fitted by a Gaussian function (7), with the results plotted in Figure 3, in function of the central point of the respective time interval, and using the same intervals as those used in all of the histograms of Figure 2.

$$N(t) = n_0 e^{-\left(\frac{t-\tau_X}{2\tau}\right)^2} \tag{9}$$

Here, $n_0$, $\tau_X$ and $\tau$ are the fitting parameters, with the values listed in Table 3, the $X$ subscript refers to the experiments on either eggs or adults.

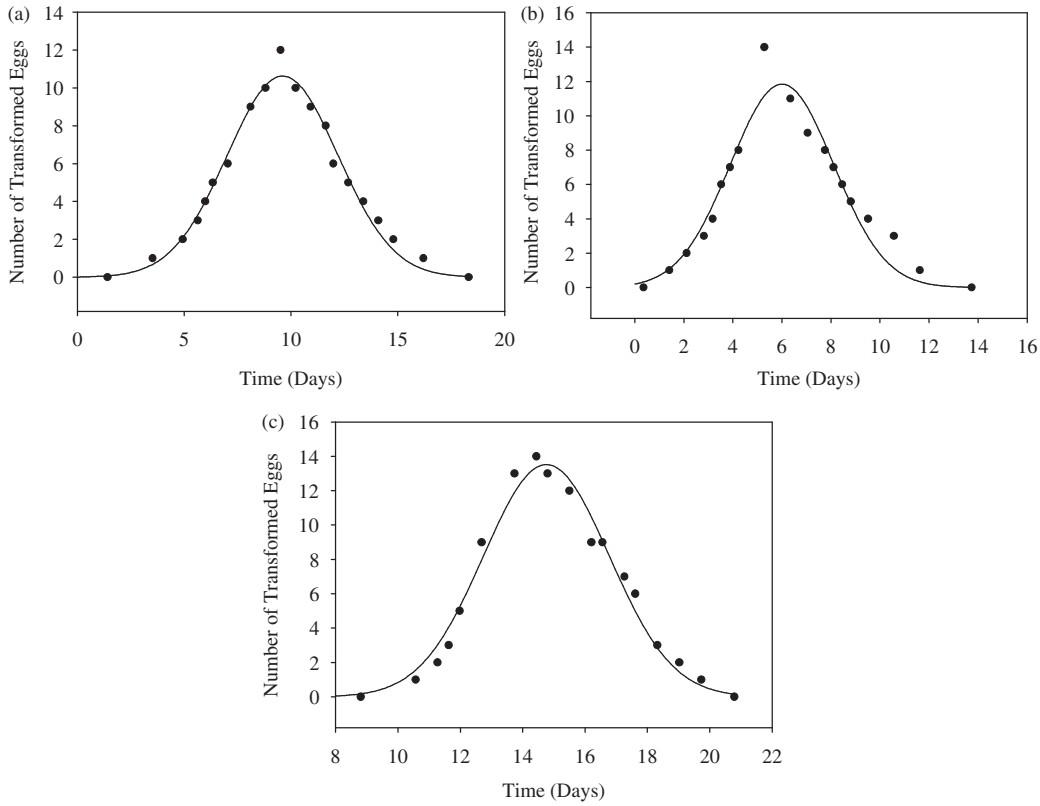


Figure 3. Time distribution of the EDP duration: (a) control experiment; (b) negative effect; (c) positive effect. Each of the experiments was reproduced three times with separate sets of *D. melanogaster* eggs. The curves show the respective Gaussian fitting functions with the parameters listed in Table 3.

Table 3. Values of Gaussian fitting parameters.

| Experiment | $N_0$ | $\tau$ (days) | $\tau_{egg}$ (days) | $\tau$ (days) (direct calculation) | $\tau_{egg}$ (days) (direct calculation) | $f$ | $p$ |
|---|---|---|---|---|---|---|---|
| (*a*) | 10.6 | 2.6 | $9.6 \pm 0.5$ | $2.4 \pm 0.2$ | $9.7 \pm 0.5$ | | – |
| (*b*) | 11.8 | 2.1 | $6.0 \pm 0.3$ | $2.2 \pm 0.2$ | $6.1 \pm 0.2$ | 0.63 | $1.3 \times 10^{-4}$ |
| (*c*) | 13.5 | 2.0 | $14.8 \pm 0.6$ | $2.1 \pm 0.2$ | $14.5 \pm 0.6$ | 1.50 | $0.6 \times 10^{-4}$ |

The $p$ column lists the probability of the null hypothesis (no difference between experiments *b*, *c* and the control experiment *a*) as calculated using the Student's *t*-test. Note that the very low values of $p$ correspond to very high statistical significance of the observed EMF effects. Refer Table 2 for the description of the experiments (*a*), (*b*) and (*c*).



The probabilities $p$ are about $10^{-4}$, thus the observed changes are highly significant. Note that similar values of $p$ were obtained for the experiments reported below, always corresponding to highly significant changes; therefore, these probability values will not be reported or discussed explicitly below. Note that the EDP duration of the control egg sets is in acceptable agreement with the results obtained earlier (Bozcuk, 1978; King, 1970).

Since the relationship (9) is an approximate description of data distribution, we also carried out direct calculations of $\tau_X$ and $\tau$ parameter values and of their uncertainties, using the standard statistical approach. The respective results are also listed Table 3, along with the EMF effect expressed as the ratio $f = \frac{\tau_X(EMF)}{\tau_X(0)}$.

## Egg experiments with 3D LFEFs and 3D LFMFs

Experiments with 3D LFEFs and 3D LFMFs were carried out in the same experimental conditions as described above. We found that turning off either electric or magnetic fields in either the P1 or P2 parameter sets resulted in negligible effects of the EMF treatment upon the EDP duration. Thus, significant effects were only produced by combined action of magnetic and electric fields of the P1 and P2 parameter sets. Noting the results obtained for *D. melanogaster* eggs, we further studied the imago longevity only for the imagoes obtained from eggs exposed to the complete P1 and P2 sets.

## Experiments on imago males

We selected 50 males produced in each of the experiments (*a*)–(*c*) on *D. melanogaster* eggs, and measured their average longevity in absence of any external fields. Each of the three experiments was reproduced 10 times on separate sets of imago males. The results are shown in Figure 4 as histograms.

These time distributions were fitted by a Gaussian function (7), with the results plotted in Figure 5 and the fitting parameters listed in Table 4.

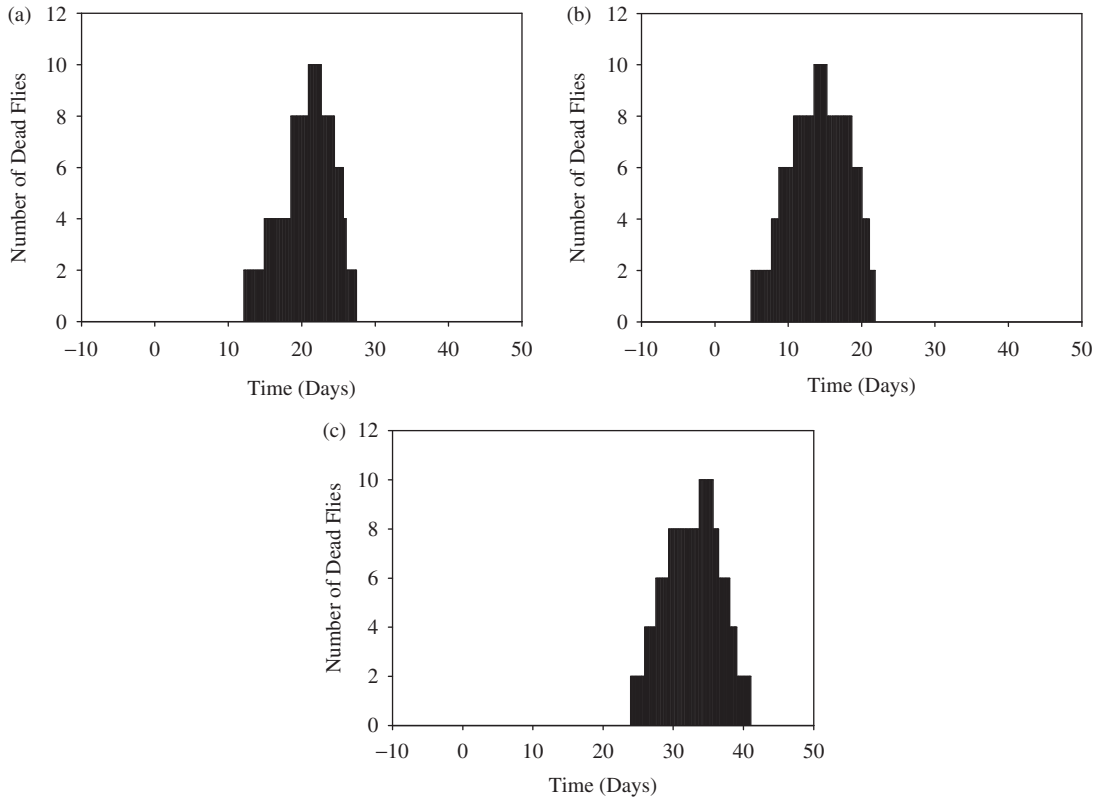


Figure 4. Time-distribution histograms of dead *D. melanogaster* males: (a) control experiment, reproduced 10 times with males produced from control sets of eggs; (b) negative effect, reproduced 10 times on males produced from eggs exposed to the field parameter set P1; (c) positive effect, reproduced 10 times on males produced from eggs exposed to the field parameter set P2.

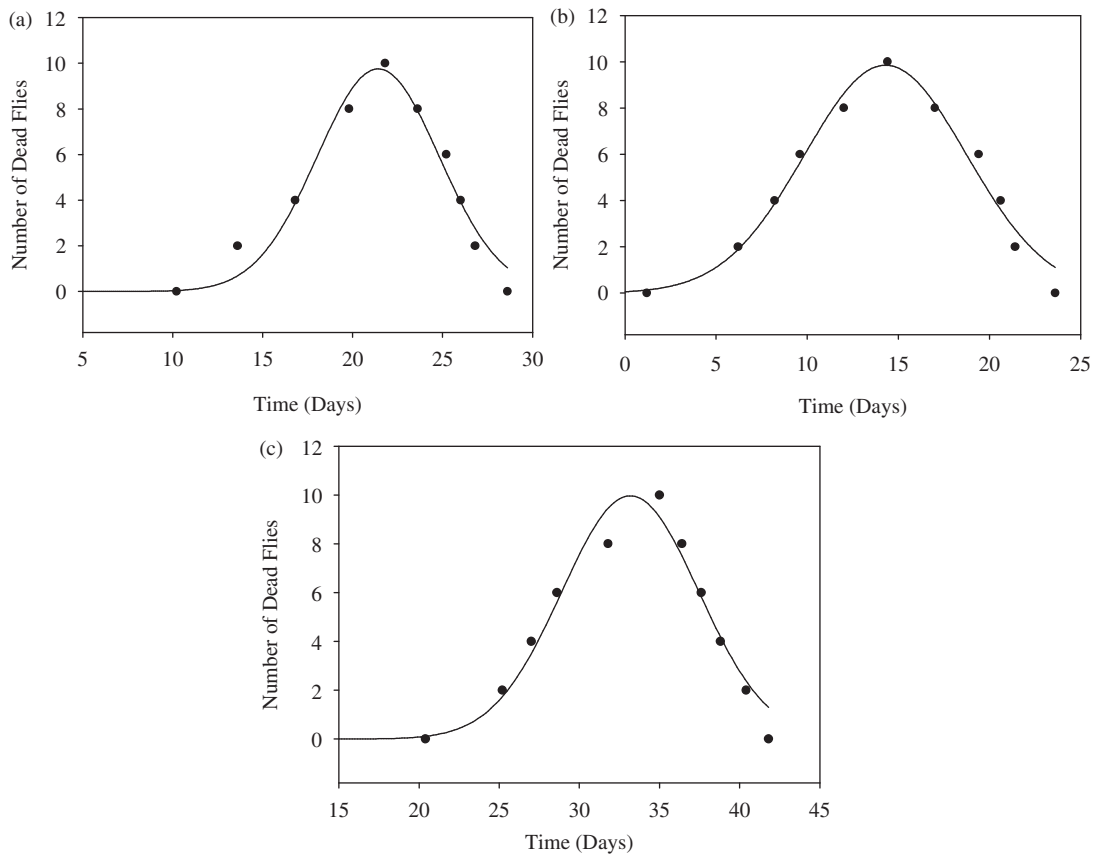


Figure 5. Time distributions of the number of dead males: (a) control experiments used males produced from eggs of experiments (*a*); (b) negative effect used males produced from eggs of experiments with the P1 field parameter set; (c) positive effect used males produced from eggs of experiments with the P2 field parameter set. Each type of experiment was reproduced 10 times on separate sets of males. The curves show the respective Gaussian fitting functions with the parameters listed in Table 4.

Table 4. Values of the Gaussian fitting and of the directly calculated parameters.

| Experiment | $n_0$ | $\tau$ (days) | $\tau_{ad}$ (days) | $\tau_{ad}$ (days; exposed as imagoes: Makarov and Khmelinskii, 2013) | $p$ | $\tau$ (days; direct calculation) | $\tau_{ad}$ (days; direct calculation) | $f$ |
|---|---|---|---|---|---|---|---|---|
| (*a*) | 9.8 | 3.39 | $21.41 \pm 0.56$ | $17.81 \pm 0.40$ | – | $3.27 \pm 0.21$ | $21.33 \pm 0.53$ | – |
| (*b*) | 9.8 | 4.45 | $14.29 \pm 0.31$ | $14.32 \pm 0.26$ | $0.9 \times 10^{-4}$ | $4.41 \pm 0.24$ | $14.31 \pm 0.34$ | 0.67 |
| (*c*) | 10.0 | 4.27 | $33.18 \pm 0.61$ | $25.56 \pm 0.50$ | $0.8 \times 10^{-4}$ | $4.22 \pm 0.23$ | $33.22 \pm 0.62$ | 1.57 |

Refer Table 2 for the description of the experiments (*a*), (*b*) and (*c*). We believe the difference with our previous results in the control experiment (*a*) is due to the presently implemented change in the imago selection procedure.

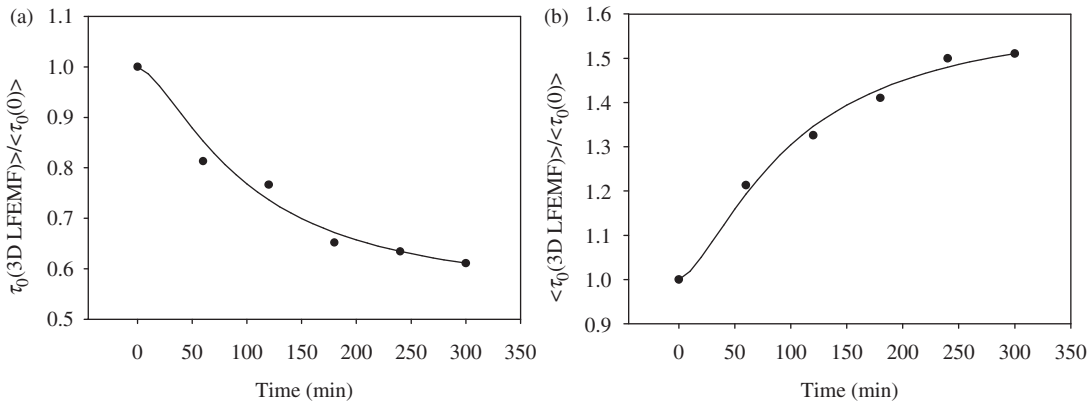


Figure 6. Normalized average egg-to-imago development period duration $<\tau_0(3D\ LFEMF)>/<\tau_0(0)>$ in function of the exposure time of the *D. melanogaster* eggs: (a) P1 field parameter set, producing a negative effect and (b) P2 field parameter set, producing a positive effect.

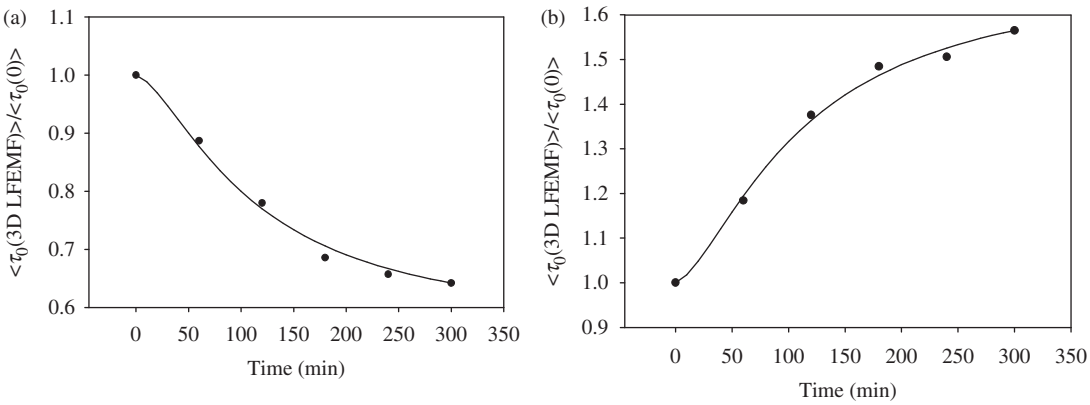


Figure 7. Normalized average imago longevity period $<\tau_0(3D\ LFEMF)>/<\tau_0(0)>$ in function of the exposure time for *D. melanogaster* males produced from exposed eggs: (a) P1 field parameter set, producing a negative effect and (b) P2 field parameter set, producing a positive effect.

Table 4 also lists the imago longevity calculated directly using the modified relationship (8). The values obtained earlier in the experiments on *D. melanogaster* imagoes (Makarov and Khmelinskii, 2013) are shown in Table 4 for comparison. Notably, the longevity changes in imagoes produced from exposed eggs are significantly larger than those in imagoes exposed to the same 3D LFEMFs as adults. We interpret this result as the memory effect of the 3D LFEMF exposure, which is inherited by the respective imagoes from the exposed eggs. Later we shall discuss these results in more detail.

As we already noted, since the relationship (9) is an approximate description of the data distribution, we also carried out direct calculations of the $\tau_X$ and $\tau$ parameter values and their uncertainties using the standard statistical approach, with the respective results listed in Table 4, along with the EMF effect expressed by the ratio $f = \frac{\tau_X(EMF)}{\tau_X(0)}$.

## Effect of the exposure duration

Here, we varied the duration of the exposure to 3D LFEMFs from 0 to 5 h. The plots of the normalized effect of the 3D LFEMF exposure in function of the exposure duration for *D. melanogaster* EDP duration are shown in Figure 6 (the same statistical analysis was carried out as in other experiments; similar results were obtained and are not presented).

Note that the effects are saturated with the exposure time; extrapolated to infinite exposure time, the asymptotic relative

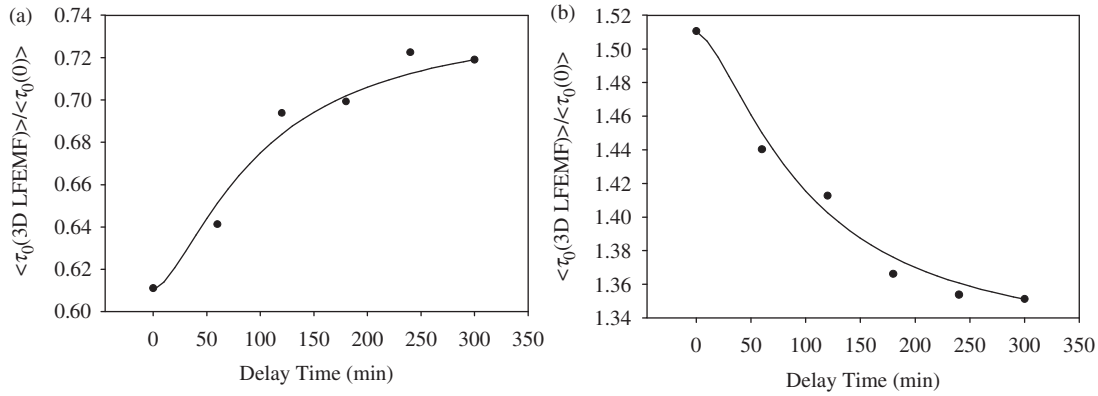


Figure 8. Normalized average egg-to-imago development period duration $<\tau_0(3D\ LFEMF)>/<\tau_0(0)>$ in function of the delay time of the exposure of *D. melanogaster* eggs: (a) P1 field parameter set, producing a negative effect and (b) P2 field parameter set, producing a positive effect.

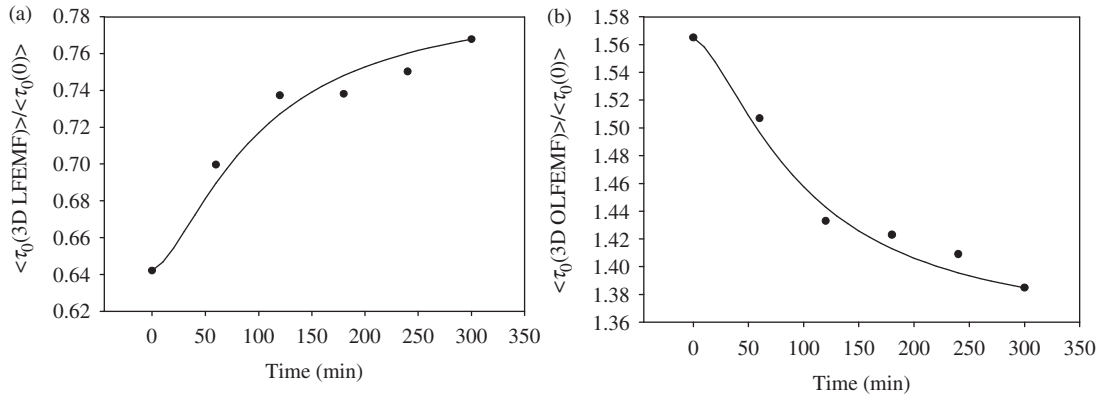


Figure 9. Average normalized imago longevity period $<\tau_0(3D\ LFEMF)>/<\tau_0(0)>$ in function of the exposure delay time for *D. melanogaster* males grown from exposed eggs: (a) P1 field parameter set, producing a negative effect and (b) P2 field parameter set, producing a positive effect.



effects are 0.53 and 1.62, respectively. Similar results obtained for *D. melanogaster* imago males produced from exposed eggs are plotted in Figure 7.

Using the data of Figure 7, we obtained the asymptotic relative values of the negative and positive effects of 0.56 and 1.70, respectively.

### Effect of the exposure delay

Here, we introduced an additional delay, varied from 0 to 5 h, before the exposure of *D. melanogaster* eggs to 3D LFEMFs was initiated. The duration of the exposure was 5 h in all of the experiments. The exposure thus started, on average, at Bownes stage 9, 10, 11, 11, and 12 for the delay of 1, 2, 3, 4 and 5 h, respectively, judging by the published development scale of unexposed eggs (Brody, 1996). Once more, no attempt was made to identify the actual development stages of the exposed eggs, although, as we already noted, the exposure always occurred within the oogenesis phase. The plots for the negative and positive effects in function of the delay time are shown in Figure 8.

Figure 8 shows that the effect of the 3D LFEMF exposure decreases with the delay time. Both plots saturate at longer delays, with the asymptotic limits of 0.73 and 1.34, respectively. Figure 9 shows similar plots obtained for *D. melanogaster* males grown from the exposed eggs.

Similarly to Figure 8, the effect on *D. melanogaster* imagoes decreases with increased delay time. Both plots saturate, with the respective asymptotic limits of 0.77 and 1.37, respectively.

### Effect of exposure substituted by delay

Here, we varied the delay time from 0 to 5 h, simultaneously varying the exposure time from 5 to 0 h. The plots of the normalized EDP are shown in Figure 10.

As expected, both plots converge to the value of 1.0 (no EMF effect) at zero exposure time. Similar plots obtained for *D. melanogaster* males grown from exposed eggs, and illustrating the memory effect, are shown in Figure 11.

As expected, both plots converge to the value of 1.0 (no EMF effect) at zero exposure time.

## Discussion

The effects of 3D LFEMFs on live systems have been recorded earlier for the yeast cells (Makarov and Khmelinskii, 2011), murine retinal cells (Makarov, 2013) and *D. melanogaster* imagoes (Makarov and Khmelinskii, 2013). Earlier we found (Makarov and Khmelinskii, 2013) that external 3D LFEMFs may either increase or reduce the *D. melanogaster* longevity. Here, we made similar experiments on *D. melanogaster* eggs and imagoes grown from exposed eggs.

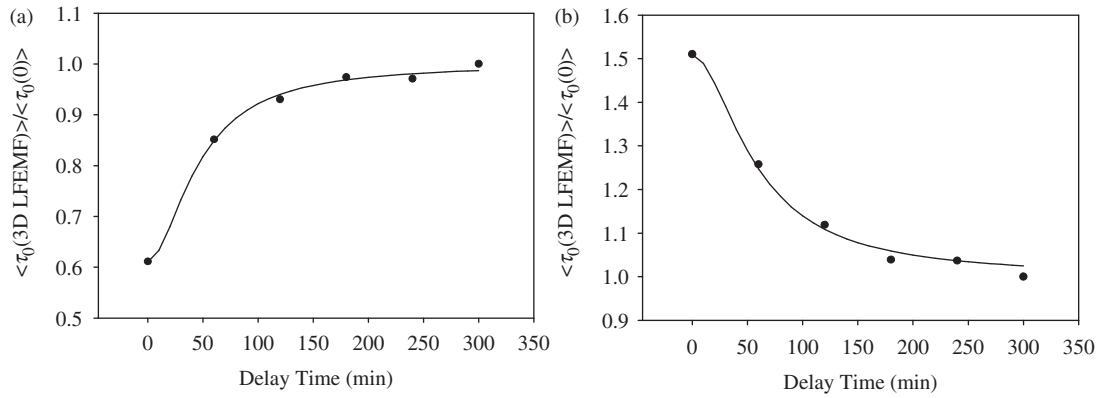


Figure 10. Average normalized EDP duration $<\tau_0(3D\ LFEMF)>/<\tau_0(0)>$ in function of the delay time (exposure time = 5 h less the delay time) for *D. melanogaster* eggs: (a) P1 field parameter set, producing a negative effect and (b) P2 field parameter set, producing a positive effect.

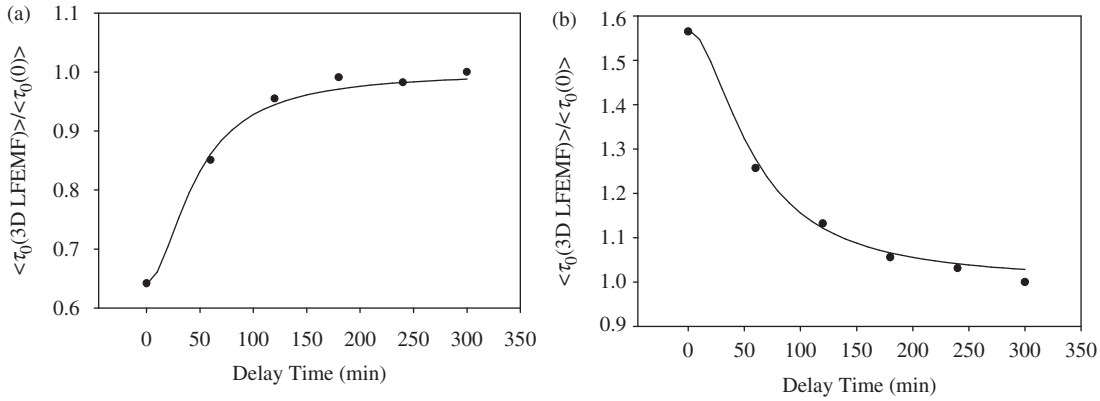


Figure 11. Plots of the normalized imago longevity period $<\tau_0(3D\ LFEMF)>/<\tau_0(0)>$ in function of the delay time (exposure time = 5 h less the delay time) for *D. melanogaster* males grown from exposed eggs: (a) P1 field parameter set, creating a negative effect and (b) P2 field parameter set, creating a positive effect.



We believe that the mechanisms we proposed for the action of 3D LFEMFs on *D. melanogaster* imagoes (Makarov and Khmelinskii, 2013) may be used to also interpret the presently obtained results. Namely, we believe that external 3D LFEMFs may cause resonance mechanical vibrations at different spatial scales, including that of an individual live cell or of a group of cells. Similar resonance mechanical vibrations may also be induced in ion-transport chains of live cells. All of these resonance effects may affect metabolic rates in live systems.

The observed memory effects may also be interpreted in terms of the earlier proposed mechanism, where we assumed that the mechanical or charge oscillations affect the genetic and the receptor systems of the developing embryo, generating the memory of the 3D LFEMF exposure in *D. melanogaster* imagoes. As follows from the present results, the embryos are more sensitive to the action of 3D LFEMFs than the imagoes. Below we will consider some modeling approaches to the mechanistic analysis of the observed phenomena. The respective models will have to consider the development of the imago *D. melanogaster*, passing through a sequence of stages. The development stages are identified by the events taking place and the time after fertilization at which they occur. Morphogenic processes that occur from fertilization to larval hatch, with the corresponding Bownes stage number and time frame for each event, are quite well known (Campos-Ortega and Hartenstein, 1985; Colas et al., 1999; Costa et al., 1993; Driever and Nüsslein-Volhard, 1988; Foe, 1998; Foe et al., 1993; Martinez Arias, 1993; Nasiadka et al., 2002; Poulson, 1950; Sonnenblick, 1950; Tram et al., 2002). Note that we only presented a partial list of relevant references. However, several important questions remain unanswered, namely: (*a*) what stage(s) of the embryo development are the most sensitive to 3D LFEMFs; (*b*) what is the EMF action mechanism; and (*c*) what is the mechanism of the memory effect.

The mechanism of electromagnetic field action in live systems has been extensively discussed earlier (Al Ghamdi, 2012; Goodman et al., 1993; Kohane and Tiller, 2000; Lednev, 1991; Liboff, 1985, 2009, 2010; Liboff and McLeod, 1988; Panagopoulos et al., 2000, 2002, 2013; Panagopoulos, 2012; Vincze et al., 2008). They proposed that such field-induced resonance effects may be attributed to (*i*) medium polarization, (*ii*) charged particle motion in the medium; and (*iii*) charged particles moving through the membrane channels. Recalling typical polarization times of water in NaCl solutions (physiological solution), which is in the subnanosecond to picosecond time scale (Faguy and Richmond, 1996), we conclude that the electromagnetic field resonance in aqueous media should be observed in the THz frequency range, but not at low frequencies. Low-frequency polarization phenomena may only be observed for larger systems, such as

biopolymers, cell organelles, cell shape deformations etc. Disregarding the magnetic fields induced by variable electric fields, and vice versa, a model describing the ionic motion may be presented in SGS units as:

$$\frac{d^2\bar{r}}{dt^2}m+\frac{m}{\tau}\frac{d\vec{r}}{dt}=\left(q\cdot\vec{D}(t)\right)+q\left[\frac{d\vec{r}}{dt}\times\vec{B}(t)\right] \tag{10}$$

where $m$ is the effective ionic mass, $q$ is the effective ionic charge, $\boldsymbol{r}$ is the radius-vector of the ion, $\tau$ is the ionic mobility, and the periodic electric and magnetic fields are given by

$$\begin{aligned}\vec{D}(t)&=\vec{D}_0\left(e^{i\omega t}+e^{-i\omega t}\right)\\ \vec{B}(t)&=\vec{B}_0\left(e^{i\omega t}+e^{-i\omega t}\right)\end{aligned} \tag{11}$$

Equation (8) describes the ionic motion in oscillating fields; its solution has resonances at certain frequencies of the external oscillating field (cases *ii* and *iii*). The ionic drift described by Equation (10) has been analyzed in detail by Szasz and Liboff (2008). However, for the ion transport through the cellular membrane (case *iii*), such field effects should be very small due to potential differences naturally existing on the cell membrane, where the internal effective electric fields are in the kV/cm range. Therefore, it is difficult to imagine the influence of weak external fields upon ionic transport through the cellular membrane. However, we may also assume that external oscillating fields induce ionic motion in the intra-cellular medium due to modulation of its polarization.

Several authors analyzed the above model, taking into account the drift of charged particles in the presence of oscillating electric and magnetic fields. They found by solving the Equation (8) that the oscillating motion of a single charged particle shows resonance effects dependent on different system parameters (Vincze et al., 2008). The equation giving the respective frequency is similar to that describing ion cyclotron resonance (Liboff, 2009, 2010). The developed theory takes into account viscous friction (Liboff, 2009, 2010; Vincze et al., 2008), but does not include thermal diffusion, being therefore only an approximation to the more correct description.

Thus, in order to properly describe the ionic motion in liquid phase, we have to analyze the diffusion equation for ions in the presence of an external potential. Such an equation may be written as:

$$\begin{aligned}\frac{\partial n(\vec{r},t)}{\partial t}&=\hat{L}\cdot n(\vec{r},t)=-\left(\vec{\nabla}\cdot\vec{j}(\vec{r},t)\right)\\ \vec{j}(\vec{r},t)&=\vec{j}_1(\vec{r},t)+\vec{j}_2(\vec{r},t)\end{aligned} \tag{12}$$

where

$$\begin{aligned}\vec{j}_{1,i}(\vec{r},t)&=D(T)\left(\vec{\nabla}\cdot n_i(\vec{r},t)\right)\\ \vec{j}_{2,i}(\vec{r},t)&=-D(T)n_i(\vec{r},t)\cdot eZ_i\left\{\left(\vec{\nabla}\cdot\phi(t)\right)+\left[\vec{\nabla}\times\vec{A}(t)\right]\right\}\end{aligned} \tag{13}$$

Here, for an isotropic medium, $D(T)=D_0e^{-\frac{E_a}{k_BT}}$ is the temperature-dependent diffusion coefficient of the ions, $E_a$ is the effective diffusion activation energy, $k_B$ is the Boltzmann constant, $T$ is the absolute temperature, $\vec{\nabla}=\vec{i}\frac{\partial}{\partial x}+\vec{j}\frac{\partial}{\partial y}+\vec{k}\frac{\partial}{\partial z}$, $n_i(\vec{r},t)$ is the *i-th* ionic concentration, $Z_i$ is the ionic charge, $\varphi(t)$ and $\vec{A}(t)$ are the time-dependent scalar and vector potentials:

$$\begin{aligned}\varphi(\vec{r},t)&=\varphi_0\left(e^{i\left(\vec{k}\vec{r}-\omega t\right)}+e^{-i\left(\vec{k}\vec{r}-\omega t\right)}\right)\\ \vec{A}(\vec{r},t)&=\vec{A}_0\left(e^{i\left(\vec{k}'\vec{r}-\omega' t\right)}+e^{-i\left(\vec{k}'\vec{r}-\omega' t\right)}\right)\end{aligned} \tag{14}$$

The boundary conditions for Equation (12) should be additionally determined in each case of interest. Note that Equation (12) cannot be solved analytically even for one-dimensional oscillating electric or magnetic fields; therefore, we shall investigate it numerically. Note that the diffusion coefficient depends on the viscosity, differing between intra-cellular and extra-cellular mediums.

The problem may be significantly simplified, assuming that the ion is much heavier than the water molecules, thus the collisions with the latter only weakly affect the ionic trajectory. Assuming a spherical ion, we thus modify the Equation (10), to give:

$$\frac{d^2\bar{r}}{dt^2}m=\left(q\cdot\vec{D}(t)\right)+q\left[\frac{d\vec{r}}{dt}\times\vec{B}(t)\right]-6\pi\eta R\frac{d\vec{r}}{dt}\left(1+\frac{1}{6}\frac{d\vec{r}}{dt}\frac{R\rho}{\eta}\right) \tag{15}$$

where $R$ is the ion radius, $\eta$ is the viscosity coefficient and $\rho$ is the medium density. Assuming laminar motion, the latter equation may be rewritten as:

$$\frac{d^2\bar{r}}{dt^2}m=\left(q\cdot\vec{D}(t)\right)+q\left[\frac{d\vec{r}}{dt}\times\vec{B}(t)\right]-6\pi\eta(T)R\frac{d\vec{r}}{dt} \tag{16}$$

Here, the temperature dependence is included into the viscosity coefficient. The latter equation may be solved analytically for some field configurations. We analyzed Equation (16) for the following field configuration: $\boldsymbol{D}=D_x$; $\boldsymbol{B}=B_z$. In this case, Equation (16) transforms into:

$$\frac{d\upsilon_x}{dt}=\left(\frac{q}{m}\cdot D_x(t)\right)+\frac{q}{m}\left[\upsilon_y\cdot B_z(t)\right]-6\pi\eta(T)R\upsilon_x \tag{17}$$

$$\frac{d\upsilon_y}{dt}=\frac{q}{m}\left[\upsilon_x\cdot B_z(t)\right]-6\pi\eta(T)R\upsilon_y \tag{18}$$

or

$$\begin{aligned}\frac{d\left(\upsilon_x-\upsilon_y\right)}{dt}&=\left(\frac{q}{m}\cdot D_x(t)\right)-\frac{q}{m}\left[\left(\upsilon_x-\upsilon_y\right)\cdot B_z(t)\right]\\ &\quad-6\pi\eta(T)R\left(\upsilon_x-\upsilon_y\right)\\ \frac{d\upsilon_0}{dt}&=\left(D_x(t)\right)-\left[B_z(t)+6\pi\eta(T)R\right]\upsilon_0\\ &=D_{0x}Cos(\omega t)-\left(B_{0z}Cos(\omega' t)+6\pi\eta(T)R\right)\upsilon_0\\ \upsilon_0&=\frac{m}{q}\left(\upsilon_x-\upsilon_y\right)\end{aligned} \tag{19}$$

and

$$\begin{aligned}\frac{d\left(\upsilon_x+\upsilon_y\right)}{dt}&=\left(\frac{q}{m}\cdot D_x(t)\right)+\frac{q}{m}\left[\left(\upsilon_x+\upsilon_y\right)\cdot B_z(t)\right]\\ &\quad-6\pi\eta(T)R\left(\upsilon_x+\upsilon_y\right)\end{aligned} \tag{20}$$

$$\frac{d\upsilon_1}{dt} = D_{0x}Cos(\omega t) + (B_{0z}Cos(\omega' t) - 6\pi\eta(T)R)\upsilon_1$$
$$\upsilon_1 = \frac{m}{q}\left(\upsilon_x + \upsilon_y\right)$$

The solutions of these equations are given by:

$$\upsilon_0(t) = e^{-\frac{B_{0z}Cos\left(\omega' t\right)+6\pi\eta(T)R\omega' t}{\omega'}} \times D_{0x}\int_0^t Cos(\omega t') \times e^{-\frac{B_{0z}Cos\left(\omega' t'\right)+6\pi\eta(T)R\omega' t'}{\omega'}}dt'$$
$$\upsilon_1(t) = e^{-\frac{-B_{0z}Cos\left(\omega' t\right)+6\pi\eta(T)R\omega' t}{\omega'}} \times D_{0x}\int_0^t Cos(\omega t') \times e^{-\frac{-B_{0z}Cos\left(\omega' t'\right)+6\pi\eta(T)R\omega' t'}{\omega'}}dt' \quad (21)$$

The relationships (21) were analyzed numerically. We also obtained the value of the field-induced ionic current, given by:

$$I_{ion}(t) = n_{ion}\cdot q\cdot\left(Z^{(+)}\upsilon_{ion}^{(+)}(t) - Z^{(-)}\upsilon_{ion}^{(-)}(t)\right)$$
*where*
$$\upsilon_{ion}^{(\pm)}(t) = \sqrt{\upsilon_x^{(\pm)2}(t) + \upsilon_y^{(\pm)2}(t)}$$
$$\upsilon_x^{(\pm)}(t) = \frac{q}{2m}\left(\upsilon_0^{(\pm)}(t) + \upsilon_1^{(\pm)}(t)\right) \quad (22)$$
$$\upsilon_x^{(\pm)}(t) = \frac{q}{2m}\left(\upsilon_0^{(\pm)}(t) - \upsilon_1^{(\pm)}(t)\right)$$

where the subscript (±) refers to positively or negatively charged ions, $Z^{(\pm)}$ are the respective charges, $q$ is the electron charge. We applied this analysis to the field-induced current in water/glycerol mixtures with dissolved NaCl. The effective ionic radius was introduced as the Debye–Huckel (DH) radius:

$$\kappa = R_{DH} = q\sqrt{\frac{\pi I}{\varepsilon k_B T}},$$

$I$ being the ionic force; and the effective ionic mass was determined from:

$$m = \frac{1}{N}\left[\frac{\left(R_{DH}^3 - R_{Free\ Ion}^3\right)}{R_{H_2O}^3}M_{H_2O} + M_{Ion}\right] \quad (23)$$

where $R_{\text{Free Ion}}$ is the radius of a free ion, $R_{H_2O}$ is the radius of a water molecule, $M_{H_2O}$ and $M_{\text{ion}}$ are the molecular mass of $H_2O$ and atomic masses of $Na^+$ and $Cl^-$ ions, $N = 6.02\times10^{23}$ is the Avogadro number. The value of the viscosity was varied from the macroscopic viscosity of pure water (890.3 μPa s; Kestin et al., 1978) to that of glycerol (1012 mPa s; Dow Chemical Corporation, 2014), both at 25 °C. These two values correspond to low-viscosity and high-viscosity systems, and should cover the range of viscosities occurring in biological systems. Note that viscosity and the diffusion coefficient are related according to

$$D(T) = \frac{k_B T}{6\pi R_{DH}\eta(T)} \quad (24)$$

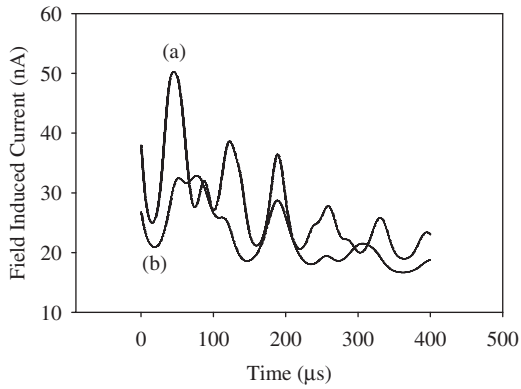


Figure 12. Time dependences of field-induced current in water (*a*) and glycerol (*b*): $D_{0x} = 12.5$ V/cm; $\omega = 17{,}000$ Hz; $D_{0x} = 11.5$ G; $\omega = 22{,}350$ Hz, temperature 25 °C, NaCl concentration of 0.05 M. Note that the scale for the trace (*b*) is expanded by a factor of 100.

which will further be used to correlate the analysis of the relationship (22) and the diffusion equation (12).

The numerical analysis was carried out for the field parameters $D_{0x} = 12.5$ V/cm; $\omega = 17{,}000$ Hz; $B_{0z} = 11.5$ G; $\omega = 22{,}350$ Hz, temperature 25 °C, NaCl concentration of 0.05 M, using both water (*a*) and glycerol (*b*) viscosities. The results are shown in Figure 12, showing that the amplitude of the field-induced current in glycerol is two orders of magnitude smaller than that in water, with the amplitude ratio of *ca*. 160. Note also the different character of current oscillations in these two media. As regards viscosity, glycerol should be closer to live systems than water, thus we expect currents below 1 nA in live cells. However, even such small currents may affect metabolism in live systems, as has been extensively discussed earlier.

An extensive discussion of the ion cyclotron resonance (ICR) induced by LFEMF in biological systems has been presented in the literature. Since the detailed mechanism of EMF action in live systems is unknown, various physiological indicators were studied, including changes in diatom motility, plant growth, rat behavior, etc. (Liboff, 2007), clinical treatment of non-unions and spinal fusion in bone (Liboff, 2006), ion parametric resonance (Blanchard and Blackman, 1994; Lednev, 1991; Vincze et al., 2008), aminoacid conductivity (Alberto et al., 2008a,b; Comisso et al., 2006; Del Giudice et al., 2002; Pazur, 2004; Zhadin et al., 1998), protein hydrolysis (Novikov and Fesenko, 2001) and stem cell differentiation (Gaetini et al., 2009). As noted by Liboff (2010), one possibility to understand EMF phenomenon is that the frequency must be specifically tuned to the unhydrated ion. However, it is quite difficult to imagine the presence of such ions in aqueous solutions. Liboff (2010) notes further that ICR-like interactions may occur between the ion and its innermost hydration shell, where the water molecules, although coupled via their dipole moments oriented radially towards the central ion within the shell, are nevertheless so rigidly constrained as to be unaffected by the Lorentz force experienced by the ion. He also notes that beyond these qualitative considerations, it has been difficult to explain exactly how the low-frequency magnetic fields tuned to ICR frequencies are so effective in producing biochemical, biological and medical effects. Furthermore,

there may have been prior unrecognized ICR-like effects in some experiments. In a number of earlier experiments where only an AC magnetic field was applied, there exists the possibility that whatever effects were observed, these were the result of a fortuitous combination of AC field in resonance with the static, but unmeasured local magnetic field. Many of the later successful ICR-like experiments have utilized the local magnetic field to supply the required magnetostatic component to achieve resonance. An examination of the charge-to-mass ratios for many biological ions, including polar amino acids, clearly shows that the ICR frequencies for these ions are in the low-frequency range when the geomagnetic field (GMF) is chosen as the static component of the resonant field combination. Liboff (2010) also noted that the significance of the fact that GMF preceded the appearance of life on earth, thereby providing an environmental template for potential biological regulatory processes, especially regarding the possible effects of magnetic field on ion transport. Among others, the effect of ultra-low-frequency MF on electro-conductivity of glutamic acid aqueous solutions was studied (Alberto et al., 2008a,b). Narrow resonance was observed in conductivity, providing an indirect proof of the external magnetic field influence on ion transport in aqueous solutions. Further on, we will analyze Equation (12) numerically.

Note also that an external EMF can affect polypeptide bond hydrolysis rates (Novikov and Fesenko, 2001). The authors proposed that resonances between the external EMF and the internal polypeptide vibrations may accelerate polypeptide bond hydrolysis. This is another mechanism, not much different from the one we proposed (Makarov and Khmelinskii, 2013) and will discuss shortly.

### Numerical analysis of Equation (12)

Using the diffusion flux of Equation (12), we define the field-induced current as:

$$I_{ion}(t) = q\left(Z^{(+)}\vec{j}^{(+)} + Z^{(-)}\vec{j}^{(-)}\right) \tag{25}$$

where $\vec{j}^{(+)}$ and $\vec{j}^{(-)}$ were determined according to Equation (12). We performed numerical analysis for the following field parameters: $D_{0x} = 12.5$ V/cm; $\omega = 17{,}000$ Hz; $B_{0z} = 11.5$ G; $\omega = 22{,}350$ Hz, temperature 25 °C, NaCl concentration of 0.05 M and glycerol viscosity. We used a home-made FORTRAN code for calculations. The diffusion coefficients for $Na^+$ and $Cl^-$ ions were taken from Equation (15), with the results obtained shown in Figure 13.

We note that the maximum field-induced current is on the sub-nA scale, while the field-induced current oscillations are not as prominent as in the previously considered example. We believe that the model including diffusion provides a better prediction for the field-induced current than the previously discussed simplified approach, though the current amplitudes have the same order of magnitude in the two cases. We therefore conclude that the model described by Equation (21) is an acceptable approximation for the analysis of field-induced currents in live systems. Note that oscillating currents may affect metabolic processes in live systems. Such currents may be induced both inside the cells and in the inter-cell

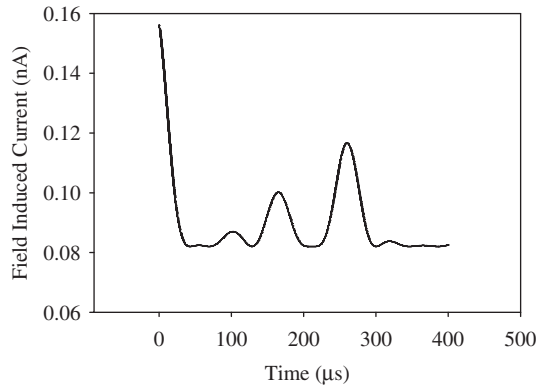


Figure 13. Time dependences of field-induced current in glycerol [Equation (11)]: $D_{0x} = 12.5$ V/cm; $\omega = 17{,}000$ Hz; $D_{0x} = 11.5$ G; $\omega = 22{,}350$ Hz, temperature 25 °C, NaCl concentration of 0.05 M.

media, affecting the transport of different molecules and ions. As we already noted, it is quite difficult to imagine field effects upon membrane transport, as the potential difference across the cell membrane is much larger than that created by the external electric fields and the induced electric fields generated by the external magnetic fields. However, the field-induced currents may affect the ion concentration gradients between the inter-cellular medium and the cellular membrane. These gradient changes may in turn affect the transport dynamics through the cellular membrane. This analysis also demonstrates the possibility of field-induced effects on ion transport. However, we cannot exclude other possible mechanisms of LFEMF effects on live systems. Then, we shall discuss some of the earlier proposed mechanisms (Makarov and Khmelinskii, 2013).

### Another mechanism of EMF effects in biological systems

Earlier we proposed (Makarov and Khmelinskii, 2011, 2013) that external LFEMF induces vibrations of (a) large fragments of biopolymer molecules with respect to each other; (b) coupled biopolymer molecules with respect to each other; (c) biopolymer molecules with respect to cellular organelles; (d) cellular organelles with respect to each other; (e) biopolymer molecules with respect to cellular membranes; (f) organelles with respect to membranes; (h) the cellular membrane as a whole; (g) entire cells with respect to each other; (i) the entire cellular ensemble as a whole, etc. A complete analysis of all possible vibrations is out of our present scope; therefore, next we shall only consider the possibilities (a) and (h).

### EMF-induced rotations of molecular fragments

Such LFEMF effects may be understood taking into account that biological activity of biopolymers is dependent on their primary, secondary and tertiary structure. The relative motion of its fragments will distort its secondary and tertiary structure, modulating its biological activity. As a model, we shall consider relative rotation of two disks connected at their common axis. The interaction potential of the relative rotation may be described by a periodic function:

$$U(\phi) = U_0(1 - Cos(N\varphi)) \tag{26}$$

where $U_0$ is the amplitude of the interaction potential, $N$ is the number of maxima for a complete turn, φ is the angle of relative rotation. The moments of inertia of the disks are $I_1$, and $I_2$, respectively. We shall assume that $I_1 << I_2$ for simplicity, the radius of the first disk being $r_0$. We shall also assume that the force created by the potential (26) is homogeneously distributed over the disk radius, and the external field-induced force described by:

$$F(t) = F_0\, Cos(\omega t) \tag{27}$$

is also homogeneously distributed over the disk radius, being normal to it and parallel to the disk surface. We shall also assume a constant force of friction $F_{\text{fric}}$, homogeneously distributed over the disk radius. The equation of motion may thus be written:

$$\frac{dM}{dt} = \frac{1}{2} r_0 F(t) - \frac{1}{2} r_0 \frac{dU}{d\phi} - \frac{1}{2} r_0 F_{fric} \tag{28}$$

simplified as:

$$\begin{aligned} 2\frac{I_1}{r_0}\frac{d^2\varphi}{dt^2} &= F_0\, Cos(\omega t) + U_0 N\, Sin(N\varphi) - F_{fric} \\ \frac{d^2\varphi}{dt^2} &= C_1\, Cos(\omega t) + C_2\, Sin(N\varphi) - C_3 \end{aligned} \tag{29}$$

where,

$$\begin{aligned} C_1 &= \frac{r_0 F_0}{2I_1} \\ C_2 &= \frac{r_0 U_0}{2I_1} \\ C_3 &= \frac{r_0 F_{fric}}{2I_1} \end{aligned} \tag{30}$$

Equation (28) cannot be solved analytically. Therefore, we analyzed the dependence of $\varphi$ vs. $\omega$ numerically, using the Runge–Kutta method (Johnson, 1968). The plots of $\varphi$ versus $\omega$ for $N = 2$, $U_0 =$ const., $F_{\text{fric}} =$ const. and different $F_0$ values are shown in Figure 14. Note that the resonant frequency, disregarding the external field-induced force and friction, is approximately given by:

$$\omega_0 = \sqrt{\frac{U_0 N}{2I_1} r_0} \propto \sqrt{\frac{U_0 N}{2mr_0}} \tag{31}$$

Taking into account typical parameter values for a biopolymer (for example, a DNA molecule) of $N = 2$ or 3, $U_0 = 0.1$–$0.2$ eV, biopolymer mass $\propto 10^5$ a.u. and the characteristic value of $r_0 = 50$ nm, we estimated the vibrational frequency $\omega_0$, obtaining the value of $(3.7 \div 4.5) \times 10^4$ Hz, which is not much different from frequencies used in our experiments. The parameters were selected so as to obtain $\omega_0 = 2.0$ arbitrary units for the numerical analysis. We note in Figure 14 that the resonance effect is infinite at $F_0 = 2$, interpreted as free rotation of disk 1 with respect to disk 2, caused by an external force. We presume that similar results may be obtained in biological systems, where field-induced rotation of a biopolymer fragment with respect to the remaining molecule may disorganize the structure of that molecule, affecting its biological activity. The interaction of external LFEMFs with a specific fragment may be caused by the existence of electric charge located on this fragment. Thus, this model provides a qualitative explanation of LFEMF action on biological systems, with such resonance phenomena capable of producing significant biological response.

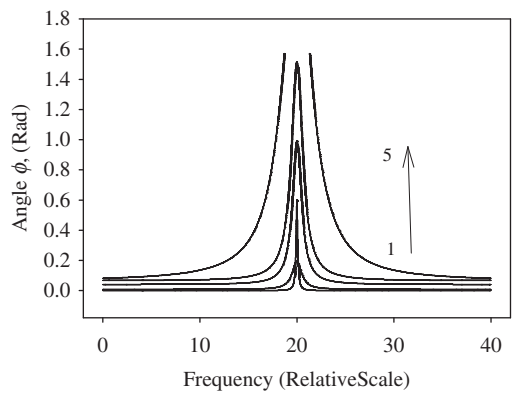


Figure 14. Dependence of $\Phi$ vs. $\omega$ for $N = 2$, and different $U_0$, $F_{\text{fric}}$ and $F_0$: (1) $F_0 = 0$, $U_0 = 1$, $F_{\text{fric}} = 0$; (2) $F_0 = 0.1$, $U_0 = 1$, $F_{\text{fric}} = 0.5$; (3) $F_0 = 0.3$, $U_0 = 1$, $F_{\text{fric}} = 0.5$; (4) $F_0 = 0.5$, $U_0 = 1$, $F_{\text{fric}} = 0.5$; (5) $F_0 = 2$, $U_0 = 1$, $F_{\text{fric}} = 0.5$. Note that all of the parameters are measured in arbitrary units.

### Cellular membrane oscillating as a whole

This model takes into account the interactions between a periodic electric field and the cellular membrane that induces cell polarization and mechanical deformation of its shape. Here, we are disregarding any effects of the magnetic fields that may further alter the deformation pattern. In this simple model the cell polarization time ($\tau_{\text{pol}}$) is much shorter than $1/\omega_{\text{EMF}}$, $\omega_{\text{EMF}}$ being the frequency of the external EMF, resulting in a mechanical motion caused by electrostatic interaction of the polarized cell with the external periodic electric field. We assume that at zero external fields the cell is spherical with radius $R$ and rigidity coefficient $k_s$. We also assume that the friction force is described by the Stokes relationship for laminar motion of a spherical object in a viscous medium. Introducing an effective mass ($m^*$) to describe the cellular shape vibrations (ellipsoid–sphere–ellipsoid), we write the respective equation of motion as:

$$\frac{d^2x}{dt^2} m^* = \frac{\alpha}{2R} D^2(t) - k_s x - 6\pi\eta(T) R \frac{dx}{dt} \tag{32}$$

This is a non-homogeneous second-order linear equation, with resonance occurring when the LFEMF frequency equals the intrinsic vibrational frequency of the entire cell as a mechanical object: $\omega_{cell} = \sqrt{\frac{k_s}{m^*}}$ . Taking into account the rigidity properties of cells (Hernández-Zapata et al., 2009), and a typical cellular mass, we estimated $\omega_{cell}$ in the range of $(1.3 \div 2.9) \times 10^4$ Hz, once more within the presently explored frequency range. We expect that such resonance effects may alter the transport of species through the cellular membrane and inside the cell, affecting cellular metabolism.

Thus, we discussed several simple models that may qualitatively account for the LFEMF effects on live systems, whereas the reality is probably significantly more complex.

## Conclusions

We believe that sub-macroscopic mechanical vibrations in *D. melanogaster* eggs created by external 3D LFEMFs significantly affect the dynamics of their metabolism. Such EMFs even more significantly affect *D. melanogaster* embryos, probably on genetic and receptor levels, producing the observed memory effects, whereby the longevity of the imagoes is affected by the exposure of the respective eggs to the 3D LFEMFs. Exposure to electromagnetic fields significantly affects the longevity of *D. melanogaster* imagoes, giving a possibility to control the life phase duration of both eggs and imagoes. We expect that similar effects may be produced in more complex live systems, including mammals and humans, with biomedical and medical applications.

## Declaration of interest

The authors report no conflicts of interest.



## References


Al Ghamdi, M. S. (2012). The effect of static electric fields on *Drosophila* behaviour. University of Southampton, Centre for Biological Sciences [Master's Thesis]. 122p. University of Southampton Research Repository ePrints Soton. Available from: http://eprints.soton.ac.uk/342464/ (accessed September 2014).

Alberto, D., Busso, L., Crotti, G., et al. (2008a). Effects of static and low-frequency alternating magnetic fields on the ionic electrolytic currents of glutamic acid aqueous solutions. *Electromagn. Biol. Med.* 27: 25–39.

Alberto, D., Busso, L., Garfagnini, R., et al. (2008b). Effects of extremely low-frequency magnetic fields on L-glutamic acid aqueous solutions at 20, 40, and 60 μT static magnetic fields. *Electromagn. Biol. Med.* 27:241–253.

Atli, E., Unlü, H. (2006). The effects of microwave frequency electromagnetic fields on the development of *Drosophila melanogaster. Int. J. Radiat. Biol.* 82:435–441.

Blanchard, J. P., Blackman, C. F. (1994). Clarification and application of an ion parametric resonance model for magnetic field interactions with biological systems. *Bioelectromagnetics* 15:217–238.

Bozcuk, A. N. (1978). The effects of some genotypes on the longevity of imago *Drosophila. Exp. Gerontol.* 13:279–286.

Brody, T. B. (1996). The interactive fly: Stages of development and mitotic domains. Available from: http://www.sdbonline.org/sites/fly/aimain/2stages.htm (accessed Dec 2013).

Campos-Ortega, J. A., Hartenstein, V. (1985). *The Embryonic Development of Drosophila melanogaster.* Berlin: Springer-Verlag.

Colas, J., Launay, J., Maroteaux, L. (1999). Maternal and zygotic control of serotonin biosynthesis are both necessary for *Drosophila germband* extension. *Mech. Dev.* 87:67–76.

Comisso, N., Del Giudice, E., De Ninno, A., et al. (2006). Dynamics of the ion cyclotron resonance effect on amino acids adsorbed at the interfaces. *Bioelectromagnetics* 27:16–25.

Costa, M., Sweeton, D., Wieschaus, E. (1993). Gastrulation in *Drosophila*: Cellular mechanisms of morphogenetic movements. In: Bate, M., Hartenstein, V. *The Development of Drosophila melanogaster.* Long Island, NY: Cold Spring Harbor Laboratories. pp. 425–465.

Dalgic, B. S. (2003). The effects of electromagnetic radiation in microwave frequency on longevity of some *Drosophila melanogaster* mutants [M.Sc. Thesis]. Ankara: Hacettepe University, The Institute for Graduate Studies in Pure and Applied Sciences.

Del Giudice, E., Fleischmann, M., Preparata, G., Talpo, G. (2002). On the ''unreasonable'' effects of ELF magnetic fields upon a system of ions. *Bioelectromagnetics* 23:522–530.

Dow Chemical Corporation. (2014). Viscosity of aqueous glycerine solutions. Available from: http://www.dow.com/optim/optim-advantage/physical-properties/viscosity.htm (accessed June 2014).

Driever, W., Nüsslein-Volhard, C. (1988). The bicoid protein determines position in the *Drosophila* embryo in a concentration-dependent manner. *Cell* 54:95–104.

Faguy, P. W., Richmond, W. N. (1996). Real-time polarization modulation infrared spectroscopy applied to the study of water and hydroxide ions at electrode surfaces. *J. Electroanal. Chem.* 410: 109–113.

Foe, V. E. (1998). Mitotic domains reveal early commitment of cells in *Drosophila* embryos. *Development* 107:1–22.

Foe, V. E., Odell, G. M., Edgar, B. A. (1993). Mitosis and morphogenesis in the drosophila embryo: Point and counterpoint. In: Bate, M., Hartenstein, V. *The Development of Drosophila melanogaster.* Long Island, NY: Cold Spring Harbor Laboratories. pp. 149–300.

Gaetini, R., Ledda, M., Barile, L., et al. (2009). Differentiation of human imago cardiac stem cells exposed to extremely low-frequency electromagnetic fields. *Cardiovasc. Res.* 82:411–420.

Goodman, R., Chizmadzhev, Y., Shirley-Henderson, A. (1993). Electromagnetic fields and cells. *J. Cell. Biochem.* 51:436–441.

Hernández-Zapata, E., Martínez-Balbuena, L., Santamaría-Holek, I. (2009). Thermodynamics and dynamics of the formation of spherical lipid vesicles. *J. Biol. Phys.* 35:297–308.

Johnson, K. J. (1968). *Numerical Methods in Chemistry.* New York/Basel: Marcel-Dekker Inc. p. 356.

Kestin, J., Sokolov, M., Wakeham, W. A. (1978). Viscosity of liquid water in the range −8 °C to 160 °C. *J. Phys. Chem.* 7:941.

King, R. C. (1970). *Ovarian Development in Drosophila melanogaster.* New York: Academic Press.

Kohane, M. J., Tiller, W. (2000). Energy, fitness, and information-augmented electromagnetic fields in *Drosophila melanogaster. J. Sci. Explorat.* 14:217–231.

Lednev, V. V. (1991). Possible mechanism for the influence of weak magnetic fields on biological systems *Bioelectromagnetics* 12: 71–5.

Liboff, A. R. (1985). Cyclotron resonance in membrane transport. In: Chiabrera, A., Nicolini, C., Schwan, H. P. *Interactions between Electromagnetic Fields and Cells*. London: Plenum Press.

Liboff, A. R. (2006). Electrical treatment of ununited bone fracture and spinal fusion. In: Webster, J. G. *Encyclopedia of Medical Devices*. 2nd edn. New York: Wiley.

Liboff, A. R. (2007). The ion cyclotron resonance hypothesis. In: Barnes, F. S., Greenebaum, B. *Handbook Bioengineering and Biophysical Aspects of Electromagnetic Fields*. 3rd ed. Boca Raton, FL: CRC Press. Chapter 9.

Liboff, A. R. (2009). Electric polarization and the viability of living systems: Ion cyclotron resonance-like interactions. *Electromagn. Biol. Med.* 28:124–134.

Liboff, A. R. (2010). A role for the geomagnetic field in cell regulation. *Electromagn. Biol. Med.* 29:105–112.

Liboff, A. R., McLeod, B. R. (1988). Kinetics of channelized membrane ions in magnetic fields. *Bioelectromagnetics* 9:39.

Makarov, V. I. (2013). Reduction of laser-induced retinal injury applying the combination of the 3D variable electric and magnetic fields in vivo. *Electromagn. Biol. Med.* 32:49–64.

Makarov, V. I., Khmelinskii, I. (2011). FTIR and UV spectroscopy in real-time monitoring of *S. cerevisiae* cell culture. *Electromagn. Biol. Med.* 30:181–197.

Makarov, V. I., Khmelinskii, I. (2013). External control of the *Drosophila melanogaster* lifespan by combination of 3D oscillating low-frequency electric and magnetic fields. *Electromagn. Biol. Med.* [Epub ahead of print]. doi: 10.3109/15368378.2013.817335.

Martinez Arias, A. (1993). Development and patterning of the larval epidermis of *Drosophila*. In: Bate, M., Hartenstein, V. *The Development of Drosophila melanogaster.* Long Island, NY: Cold Spring Harbor Laboratories. pp. 517–608.

Nasiadka, A., Dietrich, B. H., Krause, H. M. (2002). Anterior–posterior patterning in the *Drosophila* embryo. *Adv. Dev. Biol. Biochem.* 12: 156–176.

Novikov, V. V., Fesenko, E. E. (2001). Hydrolysis of some peptides and proteins in a weak combined (constant and low-frequency variable) magnetic field. *Biophysics* 46:233–238.

Onder, B. S., Bozcuk A. N. (2004). The effects of a short-term microwave exposure on the life span *Drosophila melanogaster* mutants. *Hacettepe J. Biol. Chem.* 33:111–117.

Panagopoulos, D. J. (2012). Gametogenesis, embryonic and post-embryonic development of *Drosophila melanogaster* as a modeling system for the assessment of radiation and environment toxicity. In: Spindler Barth, M. *Drosophila melanogaster Life Cycle Genetics*. Chapter I. Hauppauge, NY: Nova Science Publisher Inc.

Panagopoulos, D. J., Karabarbounis, A., Liolioussis, C. (2013). ELF alternating magnetic field decreases reproduction by DNA damage induction. *Cell. Biochem. Biophys.* 67:703–716.

Panagopoulos, D. J., Karabarbounis, A., Margaritis, L. H. (2002). Mechanism for action of electromagnetic fields on cells. *Biochem. Biophys. Res. Commun.* 298:95–102.

Panagopoulos, D. J., Karabarbounis, A., Margaritis, L. H. (2004) Effect of GSM 900-MHz mobile phone radiation on the reproductive capacity of Drosophila melanogaster. *Electromagn. Biol. Med.* 23: 29–43.

Panagopoulos, D. J., Messini, N., Karabarbounis, A., et al. (2000). A mechanism for action of oscillating electric fields on cells. *Biochem. Biophys. Res. Commun*. 272:634–640.

Pay, T. L., Andersen, F. A., Jessup, G. L. (1978). A comparative study of microwave radiation and conventional heating on the reproductive capacity of *Drosophila melanogaster. Radiat. Res.* 76: 271–282.

Pazur, A. (2004). Characterization of weak magnetic field effects in an aqueous glutamic acid solution by nonlinear dielectric spectroscopy and voltammetry. *Biomagn. Res. Technol*. 2:1–18.

Poulson, D. F. (1950). Histogenesis, organogenesis and differentiation in the embryo of *Drosophila melanogaster.* Mergen. In: Demerec, M. *Biology of Drosophila*. New York: Wiley. pp. 168–270.

Ramirez, E., Monteagudo, J. L., Garcia-Gracia, M., et al. (1983). Oviposition and development of *Drosophila* modified by magnetic fields. *Bioelectromagnetics* 4:315–326.

Roberts, D. B. (ed). (1998). *Drosophila – A Practical Approach*. 2nd ed. London: Oxford University Press.

Sonnenblick, B. P. (1950). The early embryology of *Drosophila melanogaster.* In: Demerec, M. *Biology of Drosophila*. New York: Wiley. pp. 62–167.

Szasz, V. G. A., Liboff, A. R. (2008). New theoretical treatment of ion resonance phenomena. *Bioelectromagnetics* 29:380–386.

Tipping, D. R., Chapman, K. E., Birley, A. J., et al. (1999). Observations on the effects of low frequency electromagnetic fields on cellular transcription in *Drosophila* larvae reared in field-free conditions. *Bioelectromagnetics* 20:129–131.

Tram, U., Riggs, B., Sullivan, W. (2002). Cleavage and gastrulation in *Drosophila* embryos. The cytoskeleton guides early embryogenesis in Drosophila. In: *Encyclopedia of Life Sciences*. New York: Macmillan Publishers Ltd, Nature Publishing Group. pp. 1–7.

Vincze, G., Szasz, A., Liboff, A. R. (2008). New theoretical treatment of ion resonance phenomena. *Bioelectromagnetics* 29:380–386.

Walters, E., Carstensen, E. L. (1987). Test for the effects of 60 Hz magnetic fields on fecundity and development in Drosophila. *Bioelectromagnetics* 8:351–354.

Wheeler, M. R., Clayton, F. E. (1965). A new *Drosophila* culture technique. *D. I. S.* 40:98.

Zhadin, M. N., Novikov, V. V., Barnes, F. S., Pergola, N. F. (1998). Combined action of static and alternating magnetic fields on ionic current in aqueous glutamic acid solution. *Bioelectromagnetics* 19: 41–45.